IEEE Access
Multidisciplinary | Rapid Review | Open Access Journal

Received August 18, 2017, accepted September 15, 2017, date of publication September 22, 2017,
date of current version October 25, 2017.

Digital Object Identifier 10.1109/ACCESS.2017.2755680

Enhancing the Radiation Performance of a Pyramidal Horn Antenna by Loading a Subwavelength Metasurface

XUXIANG CHEN[1], (Student Member, IEEE), AND YUEHE GE[1,2], (Member, IEEE)
[1]College of Information Science and Engineering, Huaqiao University, Xiamen 361021, China
[2]State Key Laboratory of Millimeter Waves, Southeast University, Nanjing 210096, China

Corresponding author: Yuehe Ge (yuehe@ieee.org)

This work was supported in part by the Open Research Program from the State Key Laboratory of Millimeter Waves, Nanjing, China, under Grant K201619, in part by the Foreign Cooperation Projects in Fujian Province, China, under Grant 2016I0008, and in part by the Subsidized Project for Cultivating Postgraduates' Innovative Ability in Scientific Research of Huaqiao University under Grant 1511301030.

ABSTRACT We present the detailed design and experimental demonstration of a low-sidelobe horn antenna based on controlling the amplitude and the phase distribution of the electromagnetic fields over the aperture of the horn antenna using a thin single-layer metasurface lens. The lens is composed of two identical subwavelength metallic square-ring arrays printed on the two sides of a single dielectric layer. By placing the metasurface lens inside a standard pyramidal horn, the electromagnetic fields over the horn aperture can be manipulated, resulting in low sidelobe radiation in both E- and H-planes. Both simulated and measured results demonstrate the tapered field distribution over the horn aperture and the significant reduction of sidelobes in the E-plane as well as the reduction of the backlobes.

INDEX TERMS Low-sidelobe horn, metasurface lens, square-ring arrays, tapered field distribution.

I. INTRODUCTION

Metamaterials, which are artificial materials with periodic structures in the sub-wavelength scales, have triggered great interest of developing high-performance electromagnetic devices due to their unprecedented ability of manipulating electromagnetic (EM) waves. The well-known invisibility cloaks [1]–[5] are one of the most important metamaterial applications. Other prominent metamaterial devices in various microwave applications include beam-scanning antennas [6], [7], Luneburg lens [8], Maxwell fish-eye lens [9], low sidelobes antennas [10]–[14], far-field high gain antennas [15], [16], near-field high gain antennas [17]–[20], as well as the multi-beam electromagnetic wave emission antennas [21]. Among them, most metamaterial lens antennas have served to increase the gain of antennas by converting spherical waves to plane waves using phase compensating techniques [15]–[18] or gradient refractive index (GRIN) techniques [19], [20].

The GRIN metamaterials, which first appeared in 2005 and possess the gradient equivalent permittivity and/or permeability, have been applied to the manipulation of the amplitude and phase of electromagnetic waves, resulting in a variety of electromagnetic devices, such as high-gain antennas [19], [20]. However, antennas made out of GRIN metamaterials normally have bulky structures. For example, the GRIN metamaterial lens usually have a large thickness, especially in microwave applications, because the small equivalent permittivity and/or permeability on the entire GRIN metamaterials, matching layers and hence multiple metamaterial layers or a large thickness are needed in order to achieve small reflections and the necessary phase coverage within a wide bandwidth.

Recently, metasurfaces, usually 2–D metamaterials with a planar structure, have been introduced to generate abrupt phase difference, leading to anomalous reflections and refractions. The generalized Snell Laws [22] were derived to explain these phenomena. Planar metasurfaces consist of periodic metallic structures printed on the surfaces of planar dielectric layers. Due to the various resonances including plasmonic resonances, both reflective and transmissive metasurfaces with a relatively thin thickness are capable of generating discontinuous phase shifts with high efficiency, such as focusing mirrors [13], [14], flat lens [15], [16], etc..

In this article, we propose a simple but efficient method of manipulating the aperture field by loading a thin metasurface lens inside a horn antenna, resulting in the reduction

of the radiation sidelobe level and the backlobe level. Horn antennas are widely used in various applications, for example, satellite communication systems, and serve as feeds for large parabolic reflector antennas. However, the classic pyramidal horn antennas have high sidelobes in their E plane. Much effort has been made to suppress the sidelobe levels of horn antennas. The dual-mode horns [23], corrugated horns [24], [25], horns with a solid dielectric core [26], the strip-loaded horn [27], and the recent metamaterial horns [10]–[14], were all developed for this purpose. However, these horns are usually bulky, heavy, lossy and/or more expensive. These approaches were effective but complicated when designing and manufacturing horns. The metasurface adopted here has a thin planar structure. Designed by the phase compensation method [15], [16], it is able to manipulate the phase of incident waves and hence the amplitude and phase distribution of the aperture field when placed inside the horn antenna. More specifically, placing a thin metasurface lens inside a standard pyramid horn will succeed to reduce the sidelobe level in the E plane and the backlobe level without changing its original size and increasing much the weight and the cost.

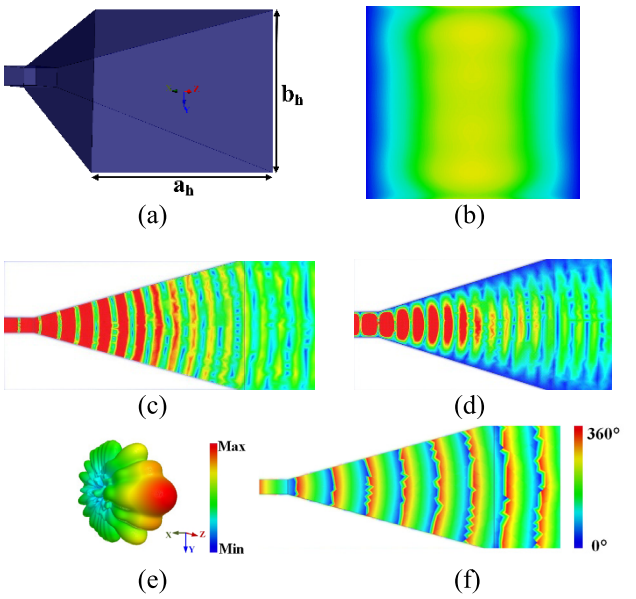

FIGURE 1. (a) The geometry of the classic airhorn, (b) Electric field amplitude distribution on the aperture plane for the airhorn, (c) The near-field amplitude distribution inside and outside the airhorn in the E plane, (d) The near-field amplitude distribution inside and outside the airhorn in the H plane, (e) 3-D radiation pattern at 12 GHz for the airhorn, (f) Electric field phase distribution for the airhorn.

II. MECHANISM OF CONTROLLING THE ELECTROMAGNETIC FIELDS

Metasurfaces having capacity to manipulate the amplitude and phase of incoming waves have attracted more and more attentions in recent years [15]–[18]. Applying arrays of metallic structures to the surface of planar dielectric slabs, which act as Huygens sources, the so called Huygens metasurfaces can be constructed. The discontinuous phase shifts can be generated on Huygens metasurfaces, resulting in the anomalous reflection and refraction. In this work, we use the Huygens metasurface to control the near fields of the antenna source, to generate the ideal aperture near-field distribution and hence enhance the radiation performance of pyramid horn antennas.

It is well known that the distributions of electromagnetic fields over the aperture of antennas play an important role in determining the far-field radiation performance. In the classic pyramidal horn antennas, the amplitude of tangential component of the aperture electromagnetic field is given by the general expressions:

$$|E_y| = E_0 \cos(\pi x/a_h) \tag{1a}$$

$$|H_x| = |E_y|/\eta \tag{1b}$$

where a_h is the aperture dimension of the pyramidal horn along the x-axis. Fig. 1(a) shows a pyramidal horn operating at 10–15 GHz, where $a_h = 103$ mm, $b_h = 83$ mm and the length of the horn is 134 mm. From Equation (1a) and (1b), one obvious feature is that the aperture distribution of electric field of a classic pyramid airhorn (the empty pyramidal horn) is approximately uniform in the E plane and tapered in the H plane, as shown in Fig. 1(b). As a result, it has high-level sidelobes in the E plane and low-level sidelobes in the H plane, due to the uniform and tapered aperture field magnitudes in the E and H planes respectively, as displayed in Fig. 1(c) and (d) respectively. Furthermore, studies have shown that the field diffracted by the E-plane edges is the main source of backlobes [28], [29].

A 3–D radiation pattern of the classical pyramidal horn antenna at 12 GHz is simulated and plotted in Fig. 1(e), which shows the low-level sidelobes in the *xoz* plane (H-plane) and relatively high-level sidelobes in the *yoz* plane (E-plane). Fig. 1(f) plots the spherical-like phase distribution inside and outside the classical pyramidal horn antenna. It has been demonstrated that the spherical-like wavefront can be manipulated by a phase compensation matesurface lens in the far field region [15], [16]. In this paper, we will show that the phase compensation metasurface lens not only can be employed to transform a spherical wave to a plane wave in the near-field region, but also can be used to tailor the amplitudes of electromagnetic fields.

Generally, the far-field radiation patterns are determined by the distributions of electromagnetic fields on the horn aperture. Therefore, an expected aperture field distribution is the key to suppress the sidelobes of the far-field radiation patterns. As shown in Fig. 2, a metasurface lens is placed inside the pyramidal horn to transform the spherical-like wave-front to be a planar wave-front. The wave-front can be further shaped so that the focusing point can be moved from the infinite region to the near-field region. Meanwhile, the radiation energies can be concentrated and hence the amplitude distributions on the horn aperture can be changed. To achieve this purpose, a metasurface lens is first designed to modify

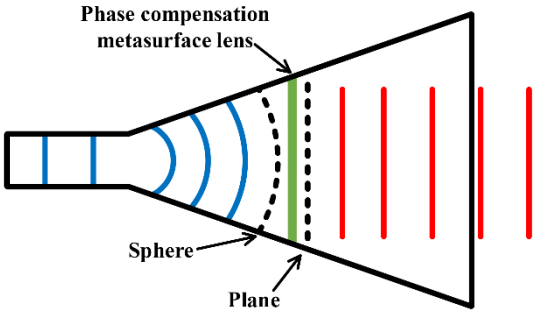

FIGURE 2. The schematic diagram of controlling the electromagnetic fields in a standard pyramidal horn.

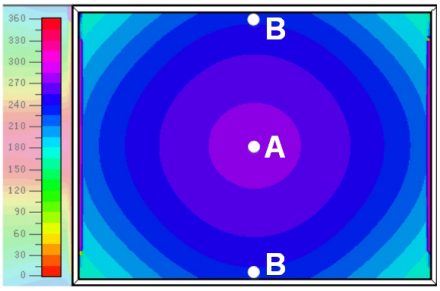

FIGURE 3. The phase distribution of the electric field on a certain cross section parallel to the horn aperture.

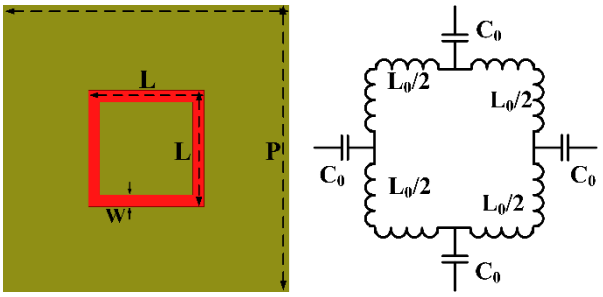

FIGURE 4. The unit element of the phase compensation metasurface lens made out of square rings and a single-layer dielectric substrate and their equivalent circuit model.

TABLE 1. The parameters of the metasurface element used in the design.

Parameter	Value
periodicity of the element: P	5mm
width of the ring: W	0.2mm
substrate thickness: t_s	3mm
copper thickness: t_p	0.035mm
substrate permittivity: $_r$	4.40
substrate loss tangent: $tan\theta$	0.02

the local phase, in order to achieve a planar near-field phase distribution inside the horn. Secondly, this lens is loaded inside the pyramidal horn antenna so that the electromagnetic wave propagating from the outside surface of the lens is able to focus on the horn aperture. The performance of the antenna depends on the location of the lens or the wave-front shaped over the horn aperture. Finally, a tapered amplitude distribution of the electric fields on the horn aperture can be achieved, which will result in low-sidelobe far-field radiation patterns. We have performed numerical simulations to obtain the phase of electric fields inside the pyramidal horn using the commercial software Ansys HFSS. Fig. 3 shows the phase distribution on a certain cross section parallel to the horn aperture, like the plane the metasurface lens located in Fig. 2. It can be seen that the phase difference between zone A and zone B is about 60°, which can be tuned to obtain a quasi-identical phase front to tailor the field distribution on the horn aperture by using a phase compensation metasurface lens, as shown in Fig. 2.

III. METASURFACE ELEMENTS

The proposed metasurface element, composed of two identical square rings printed on the two sides of a single-layer dielectric substrate, is shown in Fig. 4. The substrate uses FR4 material that has a thickness of $t_s = 3$ mm, the permittivity of $\varepsilon_r = 4.40$ and the tangent loss of $tan\theta = 0.02$. The physical parameters of the proposed element are listed in Table 1.

The unit element can be analyzed by an equivalent circuit model shown in Fig. 4. The shunt capacitance C_0 models the gap between each two adjacent square rings and the inductance L_0 represents the square ring. According to the equivalent circuit model, the resonant frequency ω_0 is calculated as

$$w_0 = \sqrt{1/L_0C_0} \tag{2}$$

The values of the inductance L_0 and capacitance C_0 depend on the geometrical parameters of the unit element. The actual side length of the inner ring varies from 2.3 mm to 3.3 mm. Consequently, the element is quite small compared to its operating wavelength (25 mm at 12 GHz) and the design frequency 12 GHz is well below its first-order resonant frequency that exhibits the characteristics of high impedance state.

Full wave numerical simulations have been carried out for the unit element to study the metasurface performance. To simulate the metasurface, a single element, shown in Fig. 4, is set in a TEM waveguide. The boundaries parallel to y direction are assigned as perfect magnetic conduct boundary conditions and those parallel to x direction are assigned as perfect electric conduct boundary conditions. If a plane wave with the electric-field polarization in the y direction illuminates the metasurface lens, the capacitors can couple to the electric field. By keeping the parameters fixed with $W = 0.2$ mm and $t_s = 3$ mm while changing L, the transmission phase characteristics are simulated and displayed in Fig. 5. It can be seen that the phase gradually reduces with increasing L. A transmission phase range of 60° can be achieved when the length of the metallic strip L varies

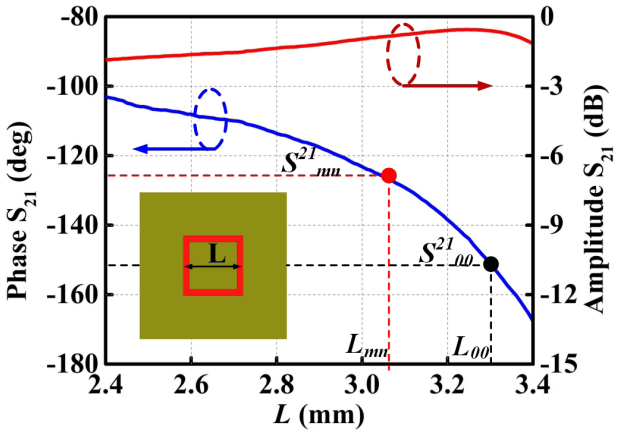

FIGURE 5. The transmission phase and coefficient versus the copper strip length (L).

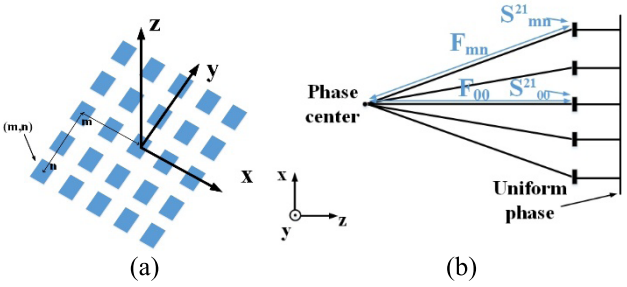

FIGURE 6. (a) The location of element (m, n), (b) The schematic diagram of the phase compensation lens.

between 2.4 mm and 3.4 mm and the transmission coefficient is less than –2 dB over the phase range. The varied phase can be used to compensate the phase of electric fields inside the pyramidal horn, which is the solid foundation of the metahorn (pyramidal horn with a metasurface lens inside), described as follows.

IV. PYRAMIDAL HORN ANTENNA WITH METASURFACE LENS

In order to reduce the sidelobe and backlobe levels of the pyramidal horn, an artificial metasurface lens is designed to adapt to the horn to modify the distribution of the aperture electric field along the *y*-axis, making the amplitude distribution tapered. We consider a metasurface lens composed of subwavelength elements with different phase characteristics. The lens consists of $M \times N$ elements, as shown in Fig. 6(a), where each element is represented by a rectangular strip. The schematic phase compensation diagram is shown in Fig. 6(b), where F_{mn} represents the phase delay between the phase center of the feed and the (m, n) element of the lens. The transmission phase across the lens at the point of (m, n) is denoted by S_{mn}^{21}. With the corresponding parameters given above, the phase distributions φ_{mn}^t and φ_{00}^t of the transmitted wave can be expressed by the following equations:

$$\varphi_{mn}^t = F_{mn} + S_{mn}^{21} \tag{3}$$

$$\varphi_{00}^t = F_{00} + S_{00}^{21} \tag{4}$$

where φ_{mn}^t and φ_{00}^t denote the phases outside the (m, n) and $(0,0)$ elements respectively. In order to obtain a constant phase front, we need

$$\varphi_{mn}^t - \varphi_{00}^t = 2k\pi, \quad k = 0, \pm 1, \ldots \tag{5}$$

Then we have

$$S_{mn}^{21} - S_{00}^{21} = -F_{mn} + F_{00} + 2k\pi, \quad k = 0, \pm 1, \ldots \tag{6}$$

When S_{00}^{21} is set to be a specific value, S_{mn}^{21} can also be obtained. Fig. 5 shows how the dimensions of square rings can be selected to achieve the required phases for compensation. Black symbol represents the original phase S_{00}^{21} versus L_{00} and red symbol denotes the proposed phase S_{mn}^{21} versus L_{mn}.

A classical pyramidal horn antenna produces a spherical-like wave front inside the horn. After loading this proposed lens, the electric field phase φ_{mn}^t on the outside surface of lens could be tuned to be quasi-identical, generating a plane wave inside the horn. Compared with the field phase distribution in a classic airhorn, shown in Fig. 1(f), a spherical-like wave is nearly converted into a plane wave and simulations have been carried out to validate the proposed design concept. Fig. 7(a) shows the proposed metahorn, where a metasurface lens is placed inside an airhorn. Through simulation studies, it is found that the performance improvement of the antenna also depends on the position of the metasurface lens. If the lens is placed near the waveguide port, the wave will propagate along the z-axis in the form of a spherical-like wave due to the flare angle of the horn antenna and there's no difference between a classic pyramidal horn and a metamaterial pyramidal horn. If the lens is placed on or close to the horn aperture, a planar phase distribution is achieved but a tapered field amplitude distribution on the horn aperture turns out to be really hard to implement. Therefore, the lens should be placed near the middle of the horn. As for our design, the lens is placed 63.9 mm away from the aperture of the horn, whose entire length is 134 mm. The phase compensation from the metasurface lens is able to manipulate the aperture field distribution to some extent and the electromagnetic energy can be concentrated to the central zone of the horn aperture. Fig. 7(b) plots the simulated field distribution over the aperture of the designed metahorn. As can be seen, the magnitudes of the electric field in the E and H planes are both tapered. Fig. 7(c) and (d) show the field distributions in the E and H planes of the metahorn. Compared with that in the E plane of the airhorn, shown in Fig. 1(c), the gradually formed tapered field distribution behind the metasurface lens is apparent and this yields the significantly reduced sidelobes and backlobes in the far field region in the E plane, as depicted in Fig. 7(e). Fig. 7(f) plots the simulated phase distribution in the E plane of the metahorn. The quasi-planar wave front is obtained on the outside surface of the metasurface lens. A direct comparison of the simulated far-field patterns both in the E and H planes between the classic airhorn and the

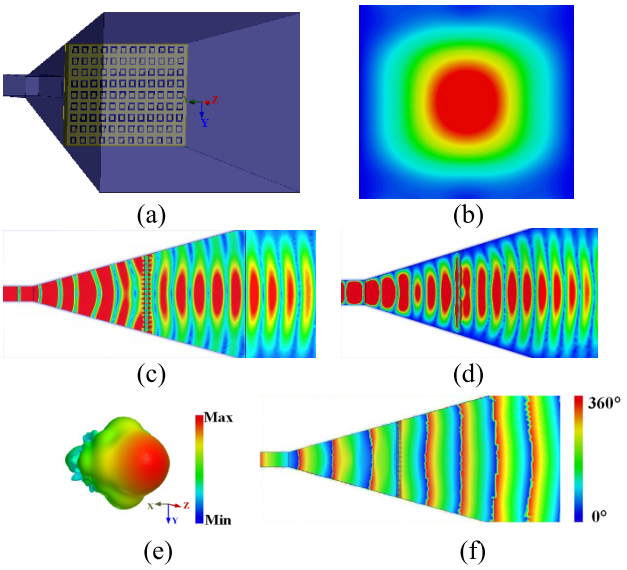

FIGURE 7. (a) The geometry of the proposed metahorn, (b) Electric field amplitude distribution on the aperture of the metahorn, (c) The near-field amplitude distribution inside and outside the metahorn in the E plane, (d) The near-field amplitude distribution inside and outside the metahorn in the H plane, (e) 3-D radiation pattern at 12 GHz for the metahorn, (f) Electric field phase distribution for the metahorn.

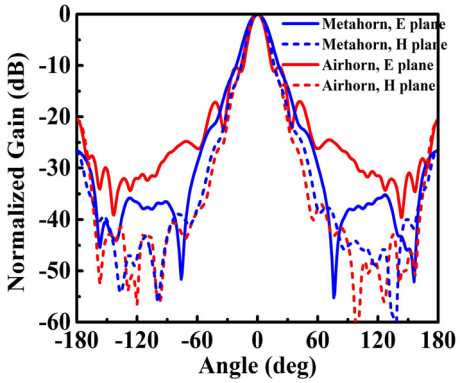

FIGURE 8. Simulated far-field patterns at 12 GHz in the E-plane and H-plane.

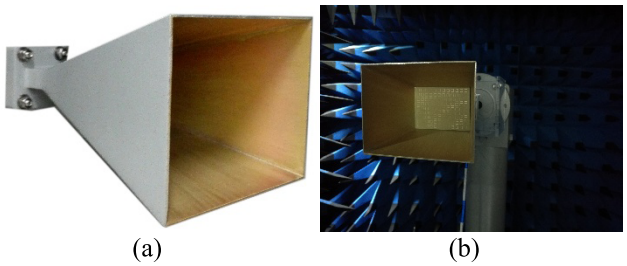

FIGURE 9. (a) The photography of the classic airhorn, (b) The metahorn antenna under test.

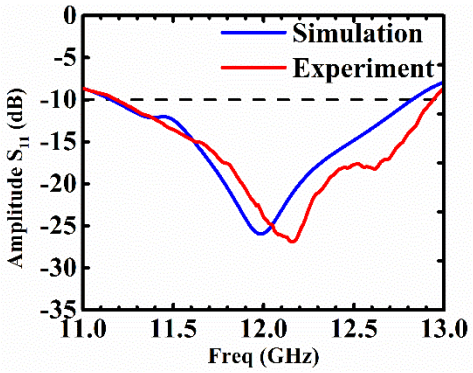

FIGURE 10. The measured and simulated reflection coefficients of the metahorn.

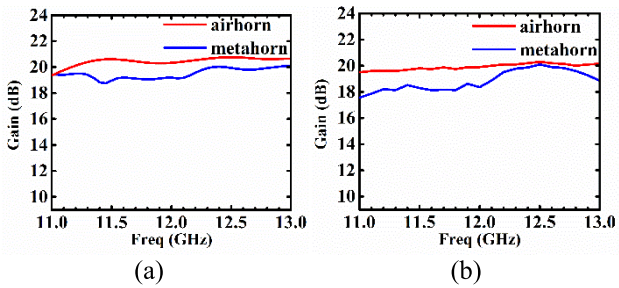

FIGURE 11. The comparison of the antenna gains for the airhorn and the metahorn. (a) Simulation, (b) Measurement.

proposed metahorn is given in Fig. 8. It can be seen clearly that the relatively lower backlobe level is obtained and the significantly lower sidelobe level is achieved in the E plane of the metahorn while the similar sidelobe level to the airhorn in the H plane of the metahorn is maintained.

V. EXPERIMENTS AND RESULTS

To further experimentally verify the design concept, the prototype of the proposed metahorn was developed. A standard gain horn LB–75–20, shown in Fig. 9(a), is used to carry out the experiments. This standard horn has an aperture size of 103×83 mm^2 and a horn length of 134 mm and operates at 10–15 GHz, with a gain range of 19–21 dBi. The typical radiation characteristics of sidelobes and backlobes, namely low-level sidelobes in the H plane and relatively high-level sidelobes in the E plane and large backlobe are also essential properties of the horn. To reduce the sidelobe level in the E plane as well as the backlobe level, a metasurface lens was designed using the unit element proposed in Section III. The standard substrate FR4 that has a dielectric constant of 4.40 and a thickness of 3 mm is applied to the design. The final lens is 60 mm long and 45 mm wide and totally contains 12×9 elements. The fabricated lens is placed inside the horn. The location is 63.9 mm away from the horn aperture. The assembled metahorn has been measured in an Anechoic Chamber. Fig. 9(b) shows the metahorn under test. Fig. 10 shows the obtained reflection coefficients both from the simulation and the measurement, which are in good agreement. According to the results, the metahorn antenna is well matched from 11.2 GHz to 12.8 GHz and the S_{11} is below –10dB within the frequency range. The gains of the

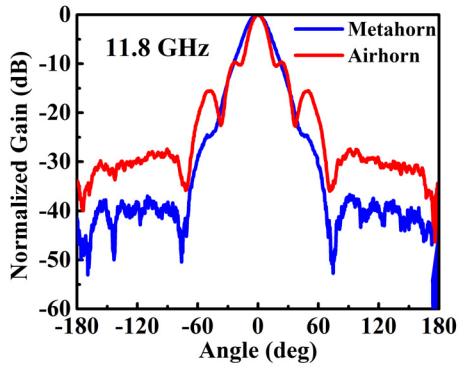

(a)

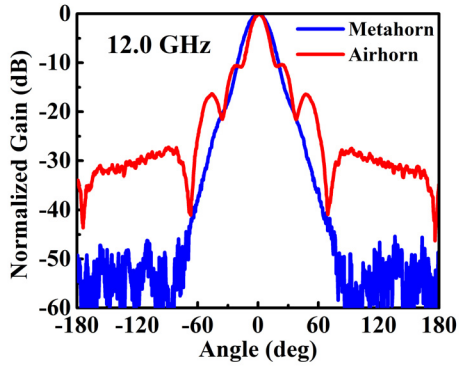

(b)

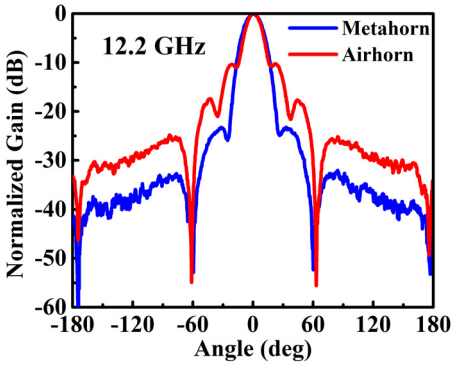

(c)

FIGURE 12. Measured far-field patterns of the airhorn and the metahorn in E-plane. (a) At 11.8 GHz, (b) At 12GHz, (c) At 12.2 GHz.

airhorn and the metahorn are plotted and compared in Fig. 11. It is clear that the gain of the airhorn is slightly higher than that of the metahorn both in simulations and in measurements. The main reason is that the aperture field of the metahorn along the *y*-axis is a tapered distribution instead of a uniform one.

The measured far-field patterns of the airhorn and metahorn at 11.8 GHz, 12 GHz and 12.2 GHz are plotted in Fig. 12(a)-(c) respectively. It can be seen that the metahorn exhibits a lower backlobe levels and lower sidelobe levels in the E plane at the three frequencies, confirming the predicted good radiation performance. Fig. 13 shows measured

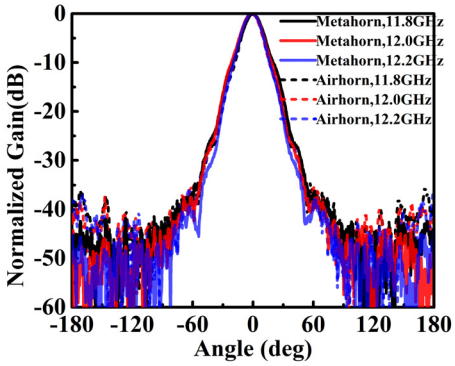

FIGURE 13. Measured far-field patterns of the airhorn and the metahorn in H-plane at 11.8 GHz, 12 GHz and 12.2 GHz.

radiation patterns in H-plane. All the sidelobe levels in the H-plane at the three frequencies are below –40 dB, almost the same as those of the airhorn. With the loading of the metasurface lens, the sidelobe level in the E-plane and the backlobe level decrease at least 15 dB, with a minor reduction of the gain over the operating band. The measured radiation patterns also show some slight asymmetry. The reason is that the mounting and the manufacturing of the lens are slightly imperfect.

VI. CONCLUSION

In summary, we have presented a method to control the amplitude and phase of electromagnetic fields inside the pyramidal horn by using a thin metasurface lens. Such a thin single-layer metasurface lens is successfully designed and placed inside of a standard pyramidal horn antenna to carry out the phase compensation and hence reduce its E-plane sidelobe level and backlobe level. According the simulated and measured results, the peak sidelobe level and the backlobe level of the original standard horn antenna have been reduced about 15 dB at the center frequency. This method can significantly enhance the radiation performance of conventional horn antennas without increasing their sizes and compromising much the weight and the cost.

REFERENCES

[1] D. Schurig, J. J. Mock, B. J. Justice, S. A. Cummer, J. B. Pendry, A. F. Starr, and D. R. Smith, "Metamaterial electromagnetic cloak at microwave frequencies," *Science*, vol. 314, no. 5801, pp. 977–980, Oct. 2006.

[2] W. Cai, U. K. Chettiar, A. V. Kildishev, and V. M. Shalaev, "Optical cloaking with metamaterials," *Nature Photon.*, vol. 1, pp. 224–227, Apr. 2007.

[3] R. Liu, C. Ji, J. J. Mock, J. Y. Chin, T. J. Cui, and D. R. Smith, "Broadband ground-plane cloak," *Science*, vol. 323, pp. 366–369, Jan. 2009.

[4] J. Valentine, J. Li, T. Zentgraf, G. Bartal, and X. Zhang, "An optical cloak made of dielectrics," *Nature Mater.*, vol. 8, pp. 568–571, Apr. 2009.

[5] H. F. Ma and T. J. Cui, "Three-dimensional broadband ground-plane cloak made of metamaterials," *Nature Commun.*, vol. 1, Jun. 2010, Art. no. 21.

[6] H. F. Ma, X. Chen, H. Sheng, X. M. Yang, W. X. Jiang, and T. J. Cui, "Experiments on high-performance beam-scanning antennas made of gradient-index metamaterials," *Appl. Phys. Lett.*, vol. 95, no. 9, p. 094107, 2009.

[7] I. Aghanejad, H. Abiri, and A. Yahaghi, "Design of high-gain lens antenna by gradient-index metamaterials using transformation optics," *IEEE Trans. Antennas Propag.*, vol. 60, no. 9, pp. 4074–4081, Sep. 2012.

[8] N. Kundtz and D. R. Smith, "Extreme-angle broadband metamaterial lens," *Nature Mater.*, vol. 9, no. 2, pp. 129–132, 2010.
[9] Z. L. Mei, J. Bai, T. M. Niu, and T. J. Cui, "A half maxwell fish-eye lens antenna based on gradient-index metamaterials," *IEEE Trans. Antennas Propag.*, vol. 60, no. 1, pp. 398–401, Jan. 2012.
[10] E. Lier, D. H. Werner, C. P. Scarborough, Q. Wu, and J. A. Bossard, "An octave-bandwidth negligible-loss radiofrequency metamaterial," *Nature Mater.*, vol. 10, no. 3, pp. 216–222, Mar. 2011.
[11] C. P. Scarborough, Q. Wu, D. H. Werner, E. Lier, R. K. Shaw, and B. G. Martin, "Demonstration of an octave-bandwidth negligible-loss metamaterial horn antenna for satellite applications," *IEEE Trans. Antennas Propag.*, vol. 61, no. 3, pp. 1081–1088, Mar. 2013.
[12] S. Shahcheraghi and A. Yahaghi, "Design of a pyramidal horn antenna with low E-plane sidelobes using transformation optics," *Prog. Electromagn. Res. M*, vol. 44, pp. 109–118, Oct. 2015.
[13] M. Q. Qi, W. X. Tang, H. F. Ma, B. C. Pan, Z. Tao, Y. Z. Sun, and T. J. Cui, "Suppressing side-lobe radiations of horn antenna by loading metamaterial lens," *Sci. Rep.*, vol. 5, Nov. 2015, Art. no. 9113.
[14] M. Q. Qi, W. X. Tang, H.-X. Xu, H. F. Ma, and T. J. Cui, "Tailoring radiation patterns in broadband with controllable aperture field using metamaterials," *IEEE Trans. Antennas Propag.*, vol. 61, no. 11, pp. 5792–5798, Nov. 2013.
[15] L.-W. Chen, Y. Ge, and T. S. Bird, "Ultrathin flat microwave transmitarray antenna for dual-polarised operations," *Electron. Lett.*, vol. 52, no. 20, pp. 1653–1654, Sep. 2016.
[16] N. Gagnon, A. Petosa, and D. A. McNamara, "Thin microwave quasi-transparent phase-shifting surface (PSS)," *IEEE Trans. Antennas Propag.*, vol. 58, no. 4, pp. 1193–1201, Apr. 2010.
[17] M. K. T. Al-Nuaimi, W. Hong, and Y. Zhang, "Design of high-directivity compact-size conical horn lens antenna," *IEEE Antennas Wireless Propag. Lett.*, vol. 13, pp. 467–470, 2014.
[18] K. Chen, Z. Yang, B. Zhu, and Y. Feng, "Gain and bandwidth enhanced patch antenna with phase compensation metasurface," in *Proc. IEEE 4th Asia–Pacific Conf. Antennas Propag. (APCAP)*, Kuta, Indonesia, Jun. 2015, pp. 267–268.
[19] Y. He, N. Ding, L. Zhang, W. Zhang, and B. Du, "Short-length and high-aperture-efficiency horn antenna using low-loss bulk anisotropic metamaterial," *IEEE Antennas Wireless Propag. Lett.*, vol. 14, pp. 1642–1645, 2015.
[20] X. Chen, H. F. Ma, X. Y. Zou, W. X. Jiang, and T. J. Cui, "Three-dimensional broadband and high-directivity lens antenna made of metamaterials," *J. Appl. Phys.*, vol. 110, no. 4, p. 044904, 2011.
[21] Z. H. Jiang, M. D. Gregory, and D. H. Werner, "Broadband high directivity multibeam emission through transformation optics-enabled metamaterial lenses," *IEEE Trans. Antennas Propag.*, vol. 60, no. 11, pp. 5063–5074, Nov. 2012.
[22] N. Yu, P. Genevet, M. A. Kats, F. Aieta, J.-P. Tetienne, F. Capasso, and Z. Gaburro, "Light propagation with phase discontinuities: Generalized laws of reflection and refraction," *Science*, vol. 334, no. 6054, pp. 333–337, Oct. 2011.
[23] J. E. Webb, "Dual mode horn antenna," U.S. Patent 3 305 870 A, Feb. 21, 1967.
[24] V. Rumsey, "Horn antennas with uniform power patterns around their axes," *IEEE Trans. Antennas Propag.*, vol. AP-14, no. 5, pp. 656–658, Sep. 1966.
[25] B. Thomas, "A method of synthesizing radiation patterns with axial symmetry," *IEEE Trans. Antennas Propag.*, vol. AP-14, no. 5, pp. 654–656, Sep. 1966.
[26] E. Lier and J. A. Aas, "Simple hybrid mode horn feed loaded with a dielectric cone," *Electron. Lett.*, vol. 21, no. 13, pp. 563–564, Jun. 1985.
[27] E. Lier and T. Schaug-Pettersen, "The strip-loaded hybrid-mode feed horn," *IEEE Trans. Antennas Propag.*, vol. Ap-35, no. 9, pp. 1086–1089, Sep. 1987.
[28] P. Russo, R. Rudduck, and L. Peters, "A method for computing E-plane patterns of horn antennas," *IEEE Trans. Antennas Propag.*, vol. AP-13, no. 2, pp. 219–224, Mar. 1965.
[29] R. E. Lawrie and P. Leon, Jr., "Corrugated horn antenna," U.S. Patent 3 631 502 A, Dec. 28, 1965.

XUXIANG CHEN (S'17) was born in Jiangsu, China, in 1992. He received the B.E. degree in electronic information engineering from Huaqiao University, Xiamen, China, in 2015, where he is currently pursuing the M.E. degree in electromagnetic field and microwave technology.

His current research interests include reconfigurable antenna, reflectarray and transmitarray, and metasurface and its applications.

Mr. Chen received the Honorable Mention Award of Student Paper Competition in the 2017 IEEE AP-S Symposium on Antennas and Propagation and USNC-URSI Radio Science Meeting.

YUEHE GE (M'02) received the B.E. and M.E. degrees from the Nanjing University of Posts and Telecommunications, China, and the Ph.D. degree in electronic engineering from Macquarie University, Sydney, Australia. From 1991 to 1999, he was an Antenna Engineer with the Nanjing Marine Radar Institute, China. From 2002 to 2011, he was a Research Fellow with the Department of Electronic Engineering, Macquarie University. Since 2011, he has been a Professor with Huaqiao University, China. He has authored or co-authored over 130 journal and conference publications and two book chapters. His research interests are in the areas of antenna theory and designs for radar and communication applications, computational electromagnetics and optimization methods, metamaterials, and their applications.

Dr. Ge is a member of the IEICE and the ACES. He received several prestigious prizes from China State Shipbuilding Corporation and China Ship Research and Development Academy, due to his contributions to China State research projects. He received the 2000 IEEE MTT-S Graduate Fellowship Awards and the 2002 Max Symons Memorial Prize of IEEE NSW Section, Australia, for the Best Student Paper. He received the 2004 Macquarie University Innovation Awards-Invention Disclosure Award. He has served as a technical reviewer for over 10 international journals and conferences.